ADVANCED MATERIALS

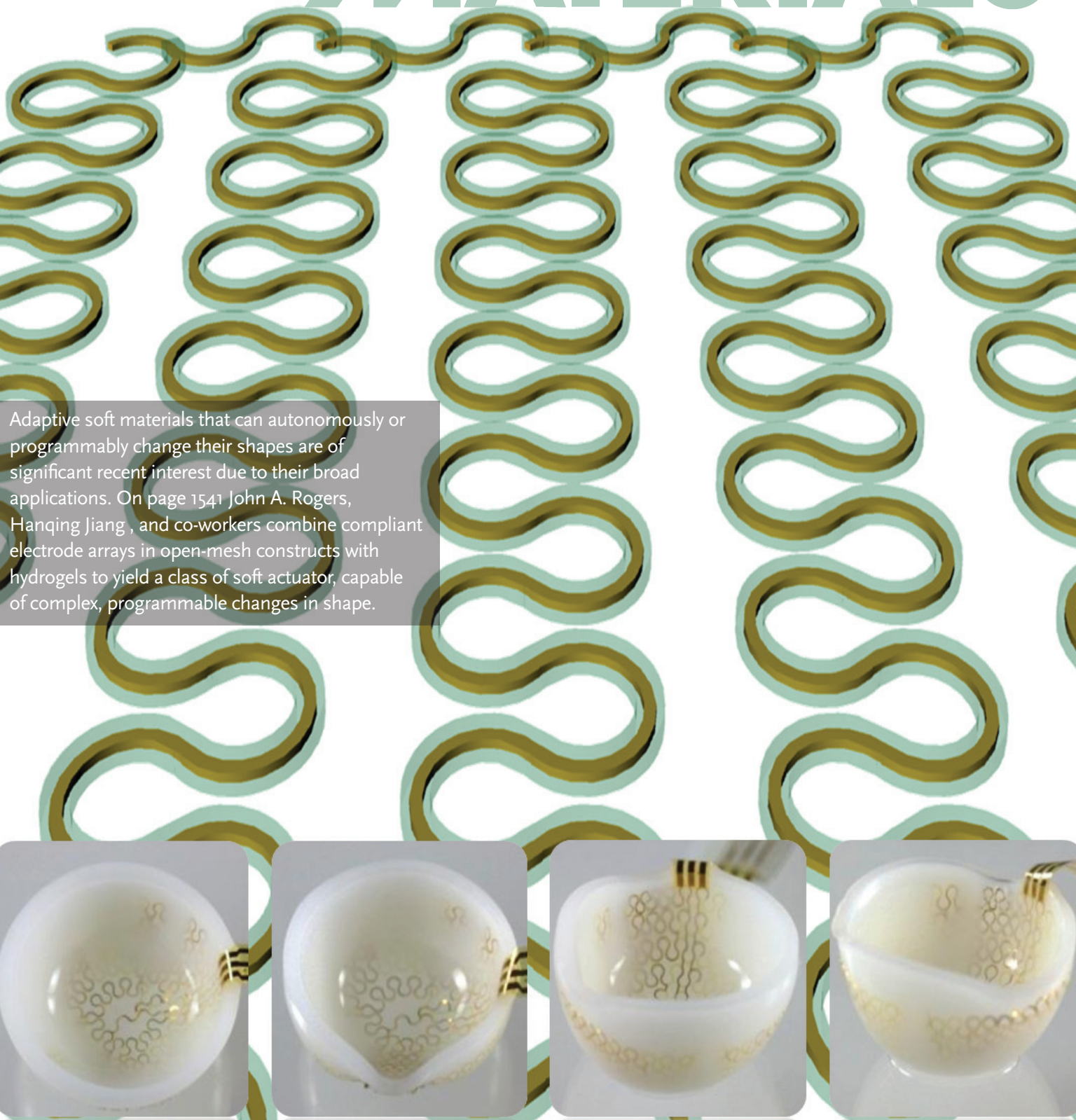

Adaptive soft materials that can autonomously or programmably change their shapes are of significant recent interest due to their broad applications. On page 1541 John A. Rogers, Hanqing Jiang , and co-workers combine compliant electrode arrays in open-mesh constructs with hydrogels to yield a class of soft actuator, capable of complex, programmable changes in shape.

WILEY-VCH

Hydrogels

Electronically Programmable, Reversible Shape Change in Two- and Three-Dimensional Hydrogel Structures

Cunjiang Yu, Zheng Duan, Peixi Yuan, Yuhang Li, Yewang Su, Xun Zhang, Yuping Pan, Lenore L. Dai, Ralph G. Nuzzo, Yonggang Huang, Hanqing Jiang, and John A. Rogers**

Adaptive soft materials that can autonomously or programmably change their shapes upon the presence of external signals or environmental cues are of significant recent interest due to their broad applications in mechanical actuators,[1–8] biomimetic robotics,[9–11] tunable photonic crystals[12–19] and other systems. Among the various materials that have been explored, hydrogels represent one of the most promising candidates, due to their ability to undergo large, reversible changes in volume upon absorbing or expelling solvents when stimulated by heat, light, pH, humidity, or electrical field. The resulting volumetric expansions/contractions[20,21] can be exploited in microfluidics,[22,23] smart lenses,[24–26] mechanical actuators,[1–8] soft robotics,[9–11] and others. In these previous demonstrations, the transformations occur globally, across the entire body of the material. By contrast, in nature, soft structures in squids, caterpillars, leaves and many other organisms actively and locally undergo changes in shape, where each element or region of the tissue deforms to some different extent, by processes of regional swelling or deswelling, thus creating localized mechanical stresses. The result provides routes to complex changes in shape and geometry, to release these internal stresses. To mimic such motions in man-made systems requires non-uniform and locally programmable levels of deformation. Several examples exist, ranging from pneumatically pumped arrays of chambers in elastomers,[27] to hybrid combinations of biological cells and soft, deformable supports,[28] to sheets of photosensitive hydrogels.[29] Each approach offers powerful capabilities, but none allows full, self-contained electronically programmable and reversible responses, of the type that might be desirable in many applications.

Though driven, spatially uniform dimensional changes in hydrogels have been reported before,[1,2] we report here the ability to program deformations in non-uniform geometries by the use of highly deformable, embedded electronics with open, serpentine mesh layouts. In examples shown in the following, the electronics provide simple, programmable patterns of localized Joule heating, to control non-uniform swelling and deswelling of the hydrogel. The results provide reversible control over diverse 3D shapes in ways that would be difficult to achieve using other approaches. We outline the materials and integration sequences, and then provide experimental examples of control schemes that can be quantitatively modeled by 3D

Dr. C. Yu, X. Zhang
Department of Materials Science and Engineering
Frederick Seitz Materials Research Laboratory
University of Illinois at Urbana-Champaign
Urbana, IL 61801, USA

Dr. Z. Duan, Y. Pan
School for Engineering of Matter, Transport and Energy
Arizona State University
Tempe, AZ 85287, USA

P. Yuan
Department of Chemistry
University of Illinois at Urbana-Champaign
Urbana, IL 61801, USA

Dr. Y. Su
Center for Mechanics and Materials
Tsinghua University
Beijing, 100084, China

Dr. Y. Li, Dr. Y. Su
Department of Civil and Environmental Engineering
and Department of Mechanical Engineering
Northwestern University
Evanston, IL 60208, USA

Prof. L. L. Dai
School for Engineering of Matter
Transport and Energy
Arizona State University
Tempe, AZ 85287, USA

Prof. R. G. Nuzzo
Department of Chemistry
and Materials Science and Engineering
Frederick Seitz Materials Research Laboratory
University of Illinois at Urbana-Champaign
Urbana, Illinois 61801, USA

Prof. Y. Huang
Department of Civil and Environmental Engineering
and Department of Mechanical Engineering
Northwestern University
Evanston, IL 60208, USA

Prof. H. Jiang
School for Engineering of Matter
Transport and Energy
Arizona State University
Tempe, AZ 85287, USA
E-mail: hanqing.jiang@asu.edu

Prof. J. A. Rogers
Department of Materials Science and Engineering
Chemistry, Mechanical Science and Engineering
Electrical and Computer Engineering
Beckman Institute for Advanced Science and Technology
and Frederick Seitz Materials
Research Laboratory
University of Illinois at Urbana-Champaign
Urbana, Illinois 61801, USA
E-mail: jrogers@illinois.edu

DOI: 10.1002/adma.201204180

finite element techniques, to capture all essential aspects of the mechanical and thermal behaviors.

The studies used thermoresponsive hydrogel poly(N-isopropylacrylamide) (pNIPAM), which is attractive due to its sharp phase transition and large swelling ratio.[30,31] The polymer chains undergo a coil (swollen) to globule (collapsed) transition at ≈33 °C,[30,32,33] known as the lower critical solution temperature (LCST). The material absorbs (expels) solvent (e.g., water) and swells (shrinks) by volume ratios as large as 260%, as the temperature decreases (increases) below (above) the LCST. The electrode meshes exploit this physics locally, by providing Joule heating in programmable patterns via external control systems. The resulting changes in shape of the hydrogel arise from a reconfiguration of the structure as some regions swell and other shrink, to release the internal stress due to these non-uniformities.

The microheaters employ designs that meet three requirements: a) strong mechanical adhesion to anchor the structures to the hydrogel, b) extreme deformability to accommodate the large and non-uniform dimensional changes associated with swelling and deswelling in the hydrogel, and c) minimal effective stiffness, to eliminate any significant mechanical constraints on the induced motions of the hydrogel. The layouts used here extend ideas developed for stretchable electronics, in which thin serpentine traces with neutral mechanical plane layouts form filaments in highly open-mesh configurations. The stretchability and compressability of such meshes follow from these structural choices, as reported extensively in other contexts.[34–37]

Figure 1a outlines the main steps for integrating such classes of deformable electronics into hydrogels. The process involves

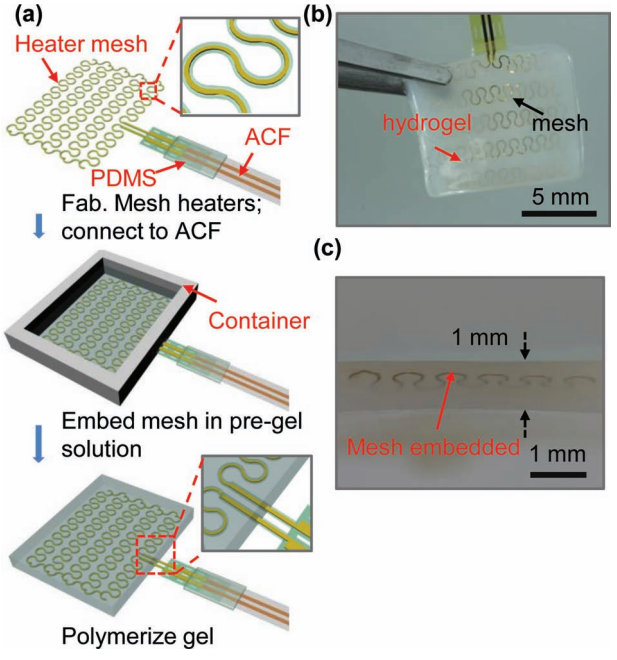

Figure 1. a) Schematic illustration of key steps for integrating an electronic system in the geometry of an open, filamentary serpentine mesh with a piece of pNIPAM hydrogel. b) Optical image of a slab of hydrogel (1 mm thick, 10 mm × 12 mm) with an embedded electroinc mesh. c) Cross-sectional view.

first fabricating thin stretchable/compressible electrode meshes on glass substrates; the devices here employ simple designs comprising trilayer stacks of polyimide (PI) (2.5 μm thick), metal (Cr (5 nm)/Au (400 nm)) and another layer of PI (2.5 μm). The layers of PI electrically isolate the metal, and also place it at the neutral mechanical plane. Details appear in the Experimental Section. Anisotropic conductive films (ACF, Elform Heat Seal Connectors), in the form of thin ribbon cables, attached to electrode pads of the mesh at one side and to a printed circuit board (PCB) at the other, provide electrical connections to external control systems. Curing the ACF at 170 °C in an oven for 20 min forms robust mechanical joints at these points of connnection. Releasing the mesh with the attached ACF cable from the glass substrate by immersion into buffered oxide etchant (BOE) (6:1 diluted) allows its manipulation for the transfer step described next. A small amount of polydimethylsiloxane (PDMS) applied at the vicinity of the ACF connection just before transfer ensures robust electrical isolation, as shown in the top image of Figure 1a.

Established forms of transfer printing,[38,39] which are in widespread use for integrating various classes of materials from source substrates onto diverse surfaces of interest, are not easily adaptable to the case of hydrogels, primarily because excessive amounts of water tend to frustrate bonding. Instead, the transfer process used here involves placing the mesh in a container with a size matched to the desired shape of the hydrogel, as illustrated in the middle frame of Figure 1a. Next, pouring a gel precursor solution into the container suspends the mesh in the liquid. Polymerization yields a solid hydrogel with the electrode mesh embedded inside, as illustrated at the bottom image of Figure 1a. The preparation details and the properties of the resulting hydrogel appear in the Experimental Section. This method for integration, combined with the exceptional high compliance of the mesh, allows free motion with the hydrogel, without any detachment or loss of adhesion. The dimensional changes that result from changes in temperature are shown in Figure S1 in the Supporting Information. Dramatic deswelling occurs between 32–34 °C, as expected,[30] with a deswelling ratio (linear dimension change) of ≈35%. Figure 1b shows a completed construct of hydrogel (≈1 mm thick) and electronic mesh, as further illustrated in Figure 1c.

Figure 2a shows an optical image of a mesh (≈11.3 mm × 9.3 mm), which can be stretched and compressed bidirectionally. Detailed geometries are presented in Figure S2 in the Supporting Information. In this particular example, the entire mesh acts as a deformable heater element, with a total resistance of ≈82 Ω. A hydrogel sheet with an embedded heater mesh is shown in Figure 2d (left). The hydrogel is ≈1 mm thick, 12 mm long, and 10 mm wide, thereby enclosing the mesh with a margin of less than 1 mm at each side. The simplicity of this design allows the mechanical influence of the mesh to be evaluated quantitatively by finite element method (FEM) simulations using the commercial package ABAQUS. As shown in Figure S3a in the Supporting Information, a 5-layer model accounts for the 1st layer of hydrogel on the top, 2nd layer of PI, 3rd layer of Au, 4th layer of PI, and 5th layer of hydrogel on the bottom; the effects of the Cr adhesion layers are neglected due to their extremely small thicknesses. Details of the simulations appear

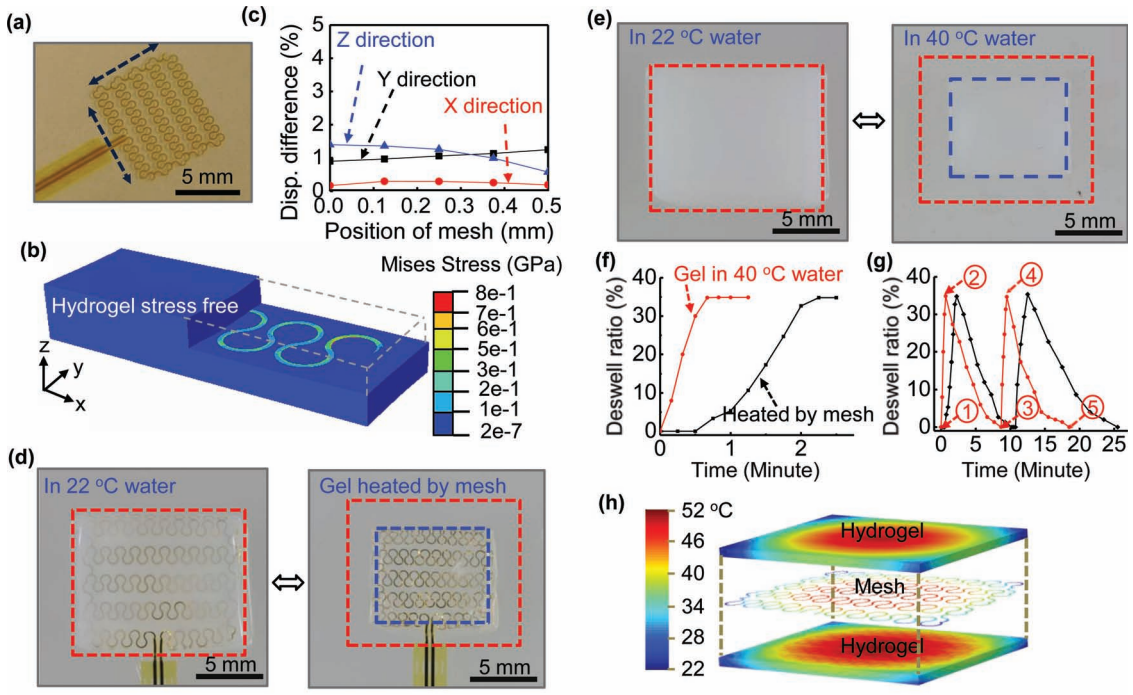

Figure 2. a) Optical image of a Joule heating structure, in an open filamentary serpentine mesh. b) FEM simulations indicate that when subjected to large thermal strains, the hydrogel remains almost stress free, even with the embedded mesh. c) Simulation results show only minor (≈1.5%) differences between displacements due to thermally induced strain for hydrogels with and without an embedded mesh. Similar results were obtained for meshes embedded at various positions (0 to 0.5 mm) through the thickness (1 mm) of the hydrogel. d) A swollen hydrogel with mesh embedded. The periphery is marked by the red dashed line (left image). Switching the heater mesh on by applying 5.2 V leads to increases in temperature, which cause the hydrogel to deswell to a size marked by the blue dashed line. The dimensions change by 35% (right image). e) A hydrogel swelled at 22 °C (left image) has the same size as the one in the left image of (d). Similar changes in dimensions occur after immersion water at 40 °C (right image). f) The dynamics of deswelling of hydrogels immersed into hot water and heated by the mesh. Deswelling to equilibrium dimensions occurs within ≈45 s after immersion in water. For actuation by the heater mesh, equilibrium occurs within 135 s for the applied voltage explored here. Both cases exhibit the same total deswelling ratio (≈35%). g) Cycling tests demonstrate reversibility in the process of deswelling/swelling. The hydrogels with and without the heater mesh are marked in red and black, respectively. The cycle starts with a swollen hydrogel, followed by deswelling and swelling again. State 1 denotes the starting point for a swollen hydrogel immersed into hot water. After immersion in water at 22 °C, the hydrogel swells to state 2. States 3, 4, and 5 represent equilibrium conditions for the second cycle. Similar experiments using the embedded heater show expected results, with good reversibility in both cases. h) FEM simulations of the temperature distribution in a hydrogel heated with an embedded mesh shown here divided at the thickness midpoint, for purposes of illustration.

in the supporting information. The model treats the strain due to swelling and deswelling as thermal strain in the hydrogel.[40] Upon application of such strain, the mesh deforms readily. Figure 2b shows the stress distribution associated with 13% compressive strain; the hydrogel remains almost stress free, which suggests that the hydrogel can deform without constraint associated with the mesh. Furthermore, the serpentine mesh layout relieves stresses in the PI and metal layers; the magnitudes of the stresses in these materials are at least two to three orders of magnitude smaller than their modulus. As additional information on the mechanics of these hybrid structures, modeling indicates that the deformations of hydrogels with and without embedded meshes are nearly the same, for identical thermal strains. In particular, as shown in Figure 2c, the differences between displacements of the hydrogel are less than 1.5% in all directions, for various configurations where the location of the mesh varies from 0 to 0.5 mm inside a 1 mm thick hydrogel. The conclusion is that the mesh can be considered as a vehicle for programming shapes in hydrogels in a way that does not alter their intrinsic mechanics.

Passing current through the mesh at a constant voltage controls the temperature of the heater and, in turn, that of the adjacent hydrogel. The relatively high density of the mesh structure ensures approximately constant temperature, via the action of thermal diffusion, over the region near the source of heat. The right image of Figure 2d shows a dramatic, isotropic decrease (≈35%) in the overall dimensions of the structure shortly after application of 5.2 V (Joule heating power of ≈0.327 W). The blue and red rectangles highlight the dimensions before and after this process. The response time is a sensitive function of the rates of thermal transport into and out of the gel and, therefore, its thickness. The time dependence of this thermally programmed deswelling appears in Figure 2f. Significant shrinkage is observed after about 30 s as the temperature reaches the LCST; the equilibrium shape occurs at ≈135 s, as marked by the black curve. The physics of the expansion/contraction in the hydrogel are such that most of the dimensional change occurs in a narrow range of temperatures near the LCST. In similar swelling experiments with bare hydrogels, illustrated in the left image of Figure 2e, a similar equilibrium is reached within

45 s after immersion in water at 40 °C water. The difference in kinetics arises simply due to the different heat sources. In both cases, the deswelling processes are reversible: switching off the current or immersing the hydrogel into cold water, returns the shape back to the original within a few minutes. As indicated in Figure 2g, tests of reversibility over a few cycles confirm this behavior. FEM simulations further verify that the temperature over most of the hydrogel is approximately uniform and is slightly higher than 40 °C, with the average value of 45.6 °C, as shown in Figure 2h. These results are consistent with observed swelling/deswelling behaviors.

The input power required for sufficient heating of the hydrogel varies with factors including: a) the area and thickness of the sample, and b) the ambient temperature. For simplicity, we assume that the Joule heating from the heaters is responsible for the uniform changes in temperature of the hydrogel and any heat dissipated, such that:

$$T = T_{\text{ambient}} + \frac{Q_{\text{heater}} - Q_{\text{loss}}}{Ah\rho C} \quad (1)$$

where T and T_{ambient} refer to the hydrogel temperature and the ambient temperature; Q_{heater} is the total amount of Joule heating produced by the mesh; Q_{loss} is the total amount of energy dissipated, including heat dissipated into the glass support and into the surrounding air. A, h, and ρ represent the area, thickness, and density of the hydrogel, and C is the specific heat capacity. The heat generated from the heater is $Q_{\text{heater}} = \frac{V^2}{R} \times t$, which corresponds to 43.8 J for the case that a 82 Ω resistor is powered by a voltage of 5.2 V for 135 s, and a total Q_{loss} of 36.3 J is obtained based on FEM simulations, where 19.9 J is dissipated into glass, and 16.4 J is removed by heat convection in air. The temperature of the hydrogel is therefore calculated to be 45.7 °C, by using an ambient temperature of 22 °C and the hydrogel parameters of dimensions (A, h), density (ρ), and specific heat capacity (C): details appear in supporting information. The calculated hydrogel temperature matches well with the averaged hydrogel temperature of 45.6 °C from simulation, and both agree with the deswelling behavior.

The simple cases presented previously illuminate the mechanics and thermal aspects, but the value in the overall approach is in its applicability to complex shapes and spatially programmable patterns of heating. A pNIPAM hydrogel in the form of a hemispherical shell, with structured heater meshes provide an example, as illustrated in Figure S5a in the Supporting Information. The fabrication involves polymerizing the hydrogel into the space between convex and concave molds, to yield a structure with inner diameter of 7 mm and outer diameter of 8 mm. Circular-shaped mesh heaters provide independent control over 5 separate sections (see **Figure 3**a). Insertion of the mesh into the hydrogel involves steps similar to those described previously, but where the convex mold serves as the container, with the concave mold as a capping structure, as demonstrated in Figure 3a and Supporting Information, Figure S5b,c. Figure 3b shows the final device. The device architectures are compatible with scaling to large numbers of independently controlled heating zones, limited mainly by the cables for external control. The integration schemes minimize spatial variations in electrode density, and associated variations in heat output. The resistances of each addressable segment

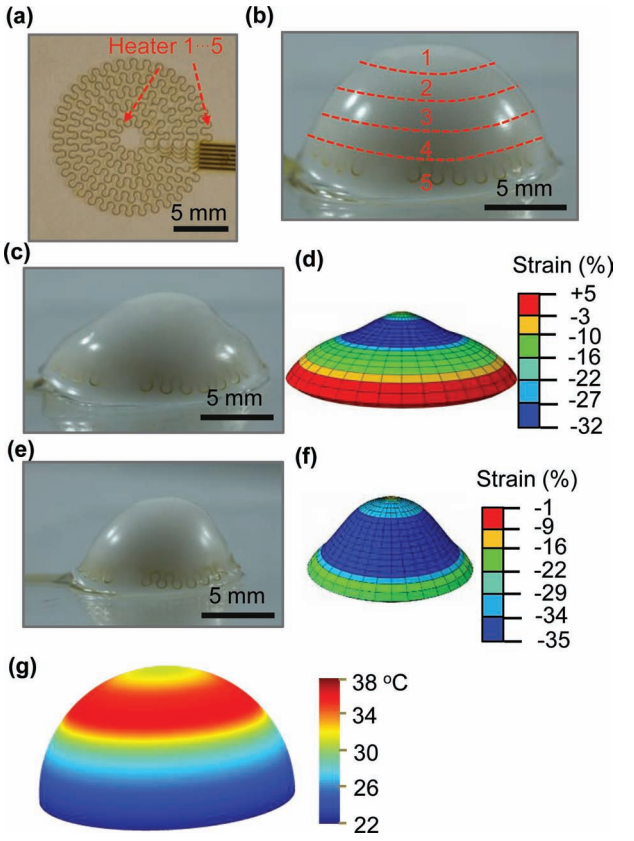

Figure 3. a) Optical image of a heater mesh, with five concentric, independently addressable regions, from inside to outside. b) Image of a hydrogel in the shape of a hemispherical shell with an embedded concentric heater mesh. c) Upon activating heaters 2 and 3, the hydrogel changes its shape as sections of 2 and 3 deswell. d) FEM simulations that capture the changes in shape observed in (c). e) Upon activating heaters 2, 3, 4, and 5, the hydrogel changes its shape as sections of 2, 3, 4, and 5 deswell. f) FEM simulations that capture the changes in shape observed in (e). g) FEM simulations of the temperature distribution after activating heaters 2 and 3 for 120 s.

of the mesh are 55, 70, 103, 118, and 130 Ω from the inner to the outer segments, respectively. As an example, activating heaters 2 and 3 leads to deswelling of the corresponding sections of the hydrogel, but in a way that leaves the largest dimension of the shell diameter, mainly determined by section 5, almost unchanged, as illustrated in Figure 3c. The overall shape returns reversibly to the one shown in Figure 3b, upon removal of the applied voltage. Similarly, by applying voltage to heaters 2–5, the corresponding sections deswell, to reduce the size and change the overall shape of the hydrogel, but without altering significantly the region near heater 1, as shown in Figure 3e. By meshing the hydrogel into brick elements and deswelling the specific sections by thermal strain, FEM simulations of such spatially controlled deswelling processes match the experiments, shown in Figure 3d and f respectively. Figure 3g illustrates simulation results of the temperature distribution after activating regions 2 and 3. The temperature of the unactivated regions remain below the LCST, such that the shape changes by deswelling regions 2 and 3 do not cause significant changes

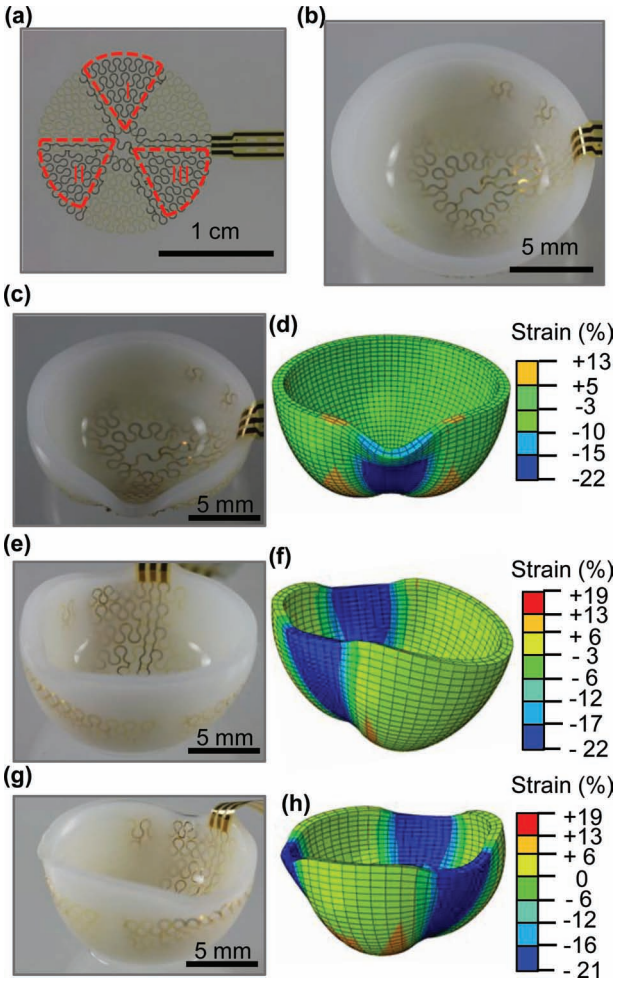

Figure 4. a) Optical image of a fan-shaped heater mesh, with separately addressable segments, marked I, II, and III. b) Image of a hydrogel in the shape of a hemispherical shell with an embedded fan-shaped heater mesh. c,e,g) Optical images of programmed shapes induced by activating one, two, and three heaters, respectively. d,f,h) FEM simulations that correspond to the experimental results shown in (c,e,g).

in the other regions. Simulations suggest that the distance from the heater to the nearest region whose temperature is lower than LCST, which defines the limits in spatial control, is ≈0.21 mm. Specifically, heat loss at the gel/air interface and thermal transport within the gel are factors that improve and degrade, respectively, the lateral resolution associated with controlled changes in shape. Further demonstrations of shape programming by selectively deswelling different sections of the hydrogel appear in Figure S6 in the Supporting Information.

Non-uniform programmable shape changes in the hemispherical pNIPAM hydrogel can be accomplished with other mesh designs. **Figure 4**a presents 3 fan-shaped heaters maintained by circular serpentine meshes, marked by I, II, and III, respectively. As indicated in Figure 4a, the heater structure involves a continuous mesh framework, metallized only in certain regions (corresponding to three fan-shaped regions in this case). This strategy provides local programmability, in a manner that simultaneously facilitates handling and integration. A hydrogel substrate with such heaters is shown in Figure 4b. The shape changes in this case arise from the deswelling of sections that support heaters. One, two, or three of the heaters can be activated selectively to achieve various shapes. Specifically, deswelling of an individual section follows from activating heater I (or II and III). Passing 44 mA current through the heater I (electrical resistance 126 Ω) for 2 min, is sufficient to increase the temperature of the corresponding section to values above the LCST, thus causing a change in the originally hemispherical shape to the one in Figure 4c. Similarly, deswelling of sections II and III yield shapes shown in Figure 4e and g, respectively. As with cases described previously, programming of these and other shapes is reversible. FEM simulations applying thermal strain in one, two and three sections yield the 3-dimensional shapes illustrated in Figure 4d, f and h. The results correspond well with the experimental observations.

In summary, integrating ultrathin compliant electronic meshes as controlling components for soft, responsive hydrogels enables reversible programming of shape in 2D and 3D. Experiments and simulations illustrate the key operational aspects of these hard/soft active materials composites. The same strategies, appropriately modified, also appear useful for nonthermal actuation, such as those that can be controlled by pH, light, or other stimuli. Application with materials other than hydrogels is also possible. We expect that such concepts could be useful in various mechanical actuators with complex shapes, biomimetic soft robotic components, and others.

Experimental Section

Fabricating the Electrode Mesh: The process began with spin-coating a 2.5 µm-thick layer of polyimide (PI) onto a temporary supporting glass slide. Following surface treatment of the PI by oxygen plasma (March RIE, plasma thermal) to improve adhesion, a 5 nm-thick layer of chrome (Cr) and a 400 nm-thick layer of gold (Au) were successively deposited by electron-beam evaporation. Spin-coating a film of photoresist (PR) (AZ 5214), patterning it by photolithography, and then wet-etching the exposed areas of the Cr/Au defined the electrode geometries. Removing the photoresist and spin-coating another 2.5 µm-thick layer of PI encapsulated the electrodes and located them at the neutral mechanical plane. A 150 nm-thick layer of SiO_2 was then deposited by plasma-enhanced chemical vapor deposition (PECVD) on the PI. This layer was patterned by reactive ion etching (RIE) (Plasma Therm) with CF_4 and O_2 gases, using PR (AZ 5214) as an etching mask. The mesh was completed by patterning the two layers of PI with an oxygen plasma, using the SiO_2 as an etching mask, and then removing the SiO_2 in 6:1 buffered oxide etchant (BOE)

Preparing the pNIPAM Hydrogel: 300 mg of N-isopropylacrylamide (NIPAM) monomer and 30 mg of methylene-N,N′-bis(acrylamide) (MBA) crosslinker were mixed and dissolved in 2 g of deionized (DI) water, with ultrasonic agitation for 10 s, and then purged with nitrogen (N_2) for 10 minutes. 8.9 mg (11.5 µL) of N,N,N',N'-tetramethylethylenediamine (TEMED) as a polymerization accelerator were added and mixed under N_2 purging. After another 10 min, 542 µL of ammonium peroxodisulfate (APS) 1% aqueous initiator solution was added and mixed thoroughly. The pre-gel solution was then dispensed into a container. The hydrogel started to polymerize within 2 to 3 min and was removed after 1 h at room temperature. Immersion into DI water for at least 24 h removed the non-polymerized monomers before any measurement or testing.

Characterizing the Properties of the Hydrogel: A 15 mm-long, 8 mm-wide, and 1 mm-thick piece of hydrogel was immersed in a water-filled container whose temperature was controlled with an external oil

bath. All three dimensions of the hydrogel were carefully characterized at each measurement temperature, after long (around 60 min) residence times to ensure equilibrium conditions. The hydrogel deswelled isotropically, with the most dramatic changes between 32 and 34 °C, consistent with the LCST for this material.[25] The data are shown in Figure S1 in the Supporting Information. A deswell ratio of >35% was achieved, as defined by:

$$\text{Deswell ratio} = (L_o - L)/L_o \times 100\% \quad (2)$$

The modulus of the dry hydrogel was measured using a dynamic mechanical analyzer (DMA) (TA Instruments, Q 800). The elastic modulus was evaluated under uniaxial tensile loading by characterizing the force versus the displacement, in samples of pNIPAM strips, 4 cm long, 5 mm wide, and 1 mm thick, stored at room temperature (22 °C) for at least 24 h on filter paper in a sealed container to dry. The dried strips were tested by clamping the two ends and applying a stepwise-increased tensile force. A tensile modulus of 0.423 MPa was obtained from the slope of the linear part of the stress–strain curve. The results were based on the average of six individual samples.

Supporting Information

Supporting Information is available from the Wiley Online Library or from the author.

Acknowledgements

H.J. and L.D. acknowledge financial support from ACS PRF 52369-ND7 and 52998-ND9. We appreciate the High Performance Computing Initiative (HPCI) at the Arizona State University. The experimental work was supported by the U.S. Department of Energy, Division of Materials Sciences under Award No. DEFG02-91ER45439, through the Frederick Seitz MRL and Center for Microanalysis of Materials at the University of Illinois at Urbana-Champaign.

Received: October 6, 2012
Published online: December 19, 2012

[1] Y. Osada, H. Okuzaki, H. Hori, *Nature* **1992**, *355*, 242.
[2] Z. B. Hu, X. M. Zhang, Y. Li, *Science* **1995**, *269*, 525.
[3] A. Richter, D. Kuckling, S. Howitz, T. Gehring, K. F. Arndt, *J. Microelectromech. Syst.* **2003**, *12*, 748.
[4] A. Sidorenko, T. Krupenkin, A. Taylor, P. Fratzl, J. Aizenberg, *Science* **2007**, *315*, 487.
[5] G. H. Kwon, Y. Y. Choi, J. Y. Park, D. H. Woo, K. B. Lee, J. H. Kim, S.-H. Lee, *Lab Chip* **2010**, *10*, 1604.
[6] X. B. Zhang, C. L. Pint, M. H. Lee, B. E. Schubert, A. Jamshidi, K. Takei, H. Ko, A. Gillies, R. Bardhan, J. J. Urban, M. Wu, R. Fearing, A. Javey, *Nano Lett.* **2011**, *11*, 3239.
[7] V. Chan, J. H. Jeong, P. Bajaj, M. Collens, T. Saif, H. Kong, R. Bashir, *Lab Chip* **2012**, *12*, 88.
[8] P. Techawanitchai, M. Ebara, N. Idota, T. A. Asoh, A. Kikuchi, T. Aoyagi, *Soft Matter* **2012**, *8*, 2844.
[9] L. Yeghiazarian, S. Mahajan, C. Montemagno, C. Cohen, U. Wiesner, *Adv. Mater.* **2005**, *17*, 1869.
[10] S. Maeda, Y. Hara, T. Sakai, R. Yoshida, S. Hashimoto, *Adv. Mater.* **2007**, *19*, 3480.
[11] J. C. Nawroth, H. Lee, A. W. Feinberg, C. M. Ripplinger, M. L. McCain, A. Grosberg, J. O. Dabiri, K. K. Parker, *Nat. Biotechnol.* **2012**, *30*, 792.
[12] K. Lee, S. A. Asher, *J. Am. Chem. Soc.* **2000**, *122*, 9534.
[13] J. D. Debord, S. Eustis, S. B. Debord, M. T. Lofye, L. A. Lyon, *Adv. Mater.* **2002**, *14*, 658.
[14] Y. Iwayama, J. Yamanaka, Y. Takiguchi, M. Takasaka, K. Ito, T. Shinohara, T. Sawada, M. Yonese, *Langmuir* **2003**, *19*, 977.
[15] L. M. Bonanno, L. A. DeLouise, *Adv. Funct. Mater.* **2010**, *20*, 573.
[16] N. Massad-Ivanir, G. Shtenberg, T. Zeidman, E. Segal, *Adv. Funct. Mater.* **2010**, *20*, 2269.
[17] C. Chen, Y. H. Zhu, H. Bao, P. Zhao, H. L. Jiang, L. M. Peng, X. L. Yang, C. Z. Li, *Soft Matter* **2011**, *7*, 915.
[18] Y. Liu, Y. X. Yuan, J. K. Ma, L. Cui, R. G. Huang, J. P. Gao, *J. Mater. Chem.* **2011**, *21*, 19233.
[19] J. T. Zhang, L. L. Wang, J. Luo, A. Tikhonov, N. Kornienko, S. A. Asher, *J. Am. Chem. Soc.* **2011**, *133*, 9152.
[20] K. Dusek, D. Patterso, *J. Polym. Sci. Part A-2: Polym. Phys.* **1968**, *6*, 1209.
[21] T. Tanaka, D. Fillmore, S. T. Sun, I. Nishio, G. Swislow, A. Shah, *Phys. Rev. Lett.* **1980**, *45*, 1636.
[22] D. J. Beebe, J. S. Moore, J. M. Bauer, Q. Yu, R. H. Liu, C. Devadoss, B. H. Jo, *Nature* **2000**, *404*, 588.
[23] D. Hlushkou, R. K. Perdue, R. Dhopeshwarkar, R. M. Crooks, U. Tallarek, *Lab Chip* **2009**, *9*, 1903.
[24] L. Dong, A. K. Agarwal, D. J. Beebe, H. Jiang, *Nature* **2006**, *442*, 551.
[25] X. Zeng, H. Jiang, *Appl. Phys. Lett.* **2008**, 93.
[26] Z. Ding, B. Ziaie, *Appl. Phys. Lett.* **2009**, 94.
[27] R. F. Shepherd, F. Ilievski, W. Choi, S. A. Morin, A. A. Stokes, A. D. Mazzeo, X. Chen, M. Wang, G. M. Whitesides, *Proc. Natl. Acad. Sci. USA* **2011**, *108*, 20400.
[28] A. W. Feinberg, A. Feigel, S. S. Shevkoplyas, S. Sheehy, G. M. Whitesides, K. K. Parker, *Science* **2007**, *317*, 1366.
[29] J. Kim, J. A. Hanna, M. Byun, C. D. Santangelo, R. C. Hayward, *Science* **2012**, *335*, 1201.
[30] H. G. Schild, *Prog. Polym. Sci.* **1992**, *17*, 163.
[31] C. Yu, Y. Pan, H. Ma, T. Ma, J. Zhang, Y. Song, M. Y. S. Kalani, L. Dai, H. Jiang, *Macromol. Rapid Commun.* **2011**, *32*, 820.
[32] M. Shibayama, T. Tanaka, *Adv. Polym. Sci.* **1993**, *109*, 1.
[33] S. Cai, Z. Suo, *J. Mech. Phys. Solids* **2011**, *59*, 2259.
[34] D.-H. Kim, Z. Liu, Y.-S. Kim, J. Wu, J. Song, H.-S. Kim, Y. Huang, K.-C. Hwang, Y. Zhang, J. A. Rogers, *Small* **2009**, *5*, 2841.
[35] D.-H. Kim, J. Viventi, J. J. Amsden, J. Xiao, L. Vigeland, Y.-S. Kim, J. A. Blanco, B. Panilaitis, E. S. Frechette, D. Contreras, D. L. Kaplan, F. G. Omenetto, Y. Huang, K.-C. Hwang, M. R. Zakin, B. Litt, J. A. Rogers, *Nat. Mater.* **2010**, *9*, 511.
[36] R.-H. Kim, D.-H. Kim, J. Xiao, B. H. Kim, S.-I. Park, B. Panilaitis, R. Ghaffari, J. Yao, M. Li, Z. Liu, V. Malyarchuk, D. G. Kim, A.-P. Le, R. G. Nuzzo, D. L. Kaplan, F. G. Omenetto, Y. Huang, Z. Kang, J. A. Rogers, *Nat. Mater.* **2010**, *9*, 929.
[37] J. Viventi, D.-H. Kim, J. D. Moss, Y.-S. Kim, J. A. Blanco, N. Annetta, A. Hicks, J. Xiao, Y. Huang, D. J. Callans, J. A. Rogers, B. Litt, *Sci. Transl. Med.* **2010**, 2.
[38] J.-H. Ahn, H.-S. Kim, K. J. Lee, S. Jeon, S. J. Kang, Y. Sun, R. G. Nuzzo, J. A. Rogers, *Science* **2006**, *314*, 1754.
[39] M. A. Meitl, Z. T. Zhu, V. Kumar, K. J. Lee, X. Feng, Y. Y. Huang, I. Adesida, R. G. Nuzzo, J. A. Rogers, *Nat. Mater.* **2006**, *5*, 33.
[40] S. Prussin, *J. Electrochem. Soc.* **1961**, *108*, C213.

ADVANCED MATERIALS

Supporting Information

for *Adv. Mater.*, DOI: 10.1002/adma.201204180

Electronically Programmable, Reversible Shape Change in Two- and Three-Dimensional Hydrogel Structures

Cunjiang Yu, Zheng Duan, Peixi Yuan, Yuhang Li, Yewang Su, Xun Zhang, Yuping Pan, Lenore L. Dai, Ralph G. Nuzzo, Yonggang Huang, Hanqing Jiang, and John A. Rogers**

Submitted to ADVANCED MATERIALS

Supporting Information for

Electronically Programmable Shape in Two and Three Dimensional Hydrogel Structures

By *Cunjiang Yu, Zheng Duan, Peixi Yuan*, Yuhang Li, Yewang Su, *Xun Zhang, Yuping Pan, Lenore Dai, Ralph G. Nuzzo, Yonggang Huang, Hanqing Jiang*,* and *John A. Rogers**

[*] Prof. John A. Rogers Corresponding-Author
Department of Materials Science and Engineering, Chemistry, Mechanical Science and Engineering, Electrical and Computer Engineering
Beckman Institute for Advanced Science and Technology, and Frederick Seitz Materials Research Laboratory
University of Illinois at Urbana-Champaign
Urbana, Illinois 61801 (USA)
E-mail: jrogers@illinois.edu
[*] Prof. Hanqing Jiang Co-corresponding-Author
School for Engineering of Matter, Transport and Energy
Arizona State University
Tempe, AZ 85287 (USA)
E-mail: hanqing.jiang@asu.edu
Prof. Yonggang Huang
Department of Civil and Environmental Engineering, and Department of Mechanical Engineering
Northwestern University
Evanston, IL 60208 (USA)
Prof. Ralph G. Nuzzo
Department of Chemistry, and Materials Science and Engineering
Frederick Seitz Materials Research Laboratory
University of Illinois at Urbana-Champaign
Urbana, Illinois 61801 (USA)
Prof. Lenore L. Dai
School for Engineering of Matter, Transport and Energy
Arizona State University
Tempe, AZ 85287 (USA)
Dr. Cunjiang Yu, Xun Zhang
Department of Materials Science and Engineering
Frederick Seitz Materials Research Laboratory
University of Illinois at Urbana-Champaign
Urbana, Illinois 61801 (USA)
Dr. Zheng Duan, Yuping Pan
School for Engineering of Matter, Transport and Energy
Arizona State University
Tempe, AZ 85287 (USA)
Peixi Yuan
Department of Chemistry
University of Illinois at Urbana-Champaign
Urbana, Illinois 61801 (USA)
Dr. Yuhang Li, Dr. Yewang Su
Department of Civil and Environmental Engineering, and Department of Mechanical Engineering

Submitted to ADVANCED MATERIALS

Northwestern University
Evanston, IL 60208 (USA)
Dr. Yewang Su
Center for Mechanics and Materials
Tsinghua University,
Beijing, China 100084

Keywords: hydrogel, programmable shape, stretchable electrode mesh, nonuniform deformation

Mechanical Analysis and Finite Element Simulations

The commercial finite element package ABAQUS was used for analysis. A three-layer model was used to calculate the effective modulus of the serpentine structure. As illustrated in Fig. S2(c), the 1st layer is PI with thickness of 2.5 μm, modulus 3.2 GPa, Poisson's ratio 0.34, modeled by 10,092 three-dimensional brick elements (C3D8 element in ABAQUS); the 2nd layer is an Au electrode, with thickness of 400 nm, modulus 79 GPa, Poisson's ratio 0.44, modeled by 10,193 C3D8 elements; the 3rd layer is the same as the 1st layer. Three layers were tied together. 8.5 waves of the serpentine (8.89 mm) were adopted in the modeling. One end of the serpentine was fixed, while the other end was subjected to a load of 0.001 N in the wavelength direction to pull the serpentine by 1.378 mm. The equivalent cross-sectional area was defined by the thickness of the serpentine (5.4 μm) times the height of the serpentine (1,038 μm). The equivalent modulus is 0.875 MPa, which is on the same order of that for hydrogels, 0.423 MPa. In other words, the serpentine has mechanical compliance similar to that of the hydrogel.

The hydrogel was modeled as a hyperelastic material and implemented in ABAQUS via its user-defined hyperelastic material (UHYPER) [1]. The principal stress σ (normalized by v/kT, where v is the specific volume of solvent molecule and kT is temperature in the unit of energy) is expressed as a function of the equilibrium swelling ratio λ_{eq},

$$\frac{\sigma v}{kT}=\frac{Nv}{\lambda_{eq}^{\ 2}}\left(\lambda_{eq}-\frac{1}{\lambda_{eq}}\right)+\ln\left(1-\frac{1}{\lambda_{eq}^{\ 3}}\right)+\frac{1}{\lambda_{eq}^{\ 3}}+\frac{\chi}{\lambda_{eq}^{\ 6}}-\frac{\mu}{kT}, \tag{S1}$$

where *Nv*, the normalized shear modulus of the dry gel, and χ, a dimensionless parameter characterizing the enthalpy of mixing, are introduced. The normalized shear modulus *Nv* can be determined by the measured tensile modulus *E* of the fully swollen gel[2]

$$Nv = \frac{\lambda_{eq}}{3}\frac{Ev}{kT}. \quad \text{(S2)}$$

For free swelling, stress σ and chemical potential μ are vanishing so that Eq. (S1) provides a means to link Flory's interaction parameter χ and equilibrium swelling ratio λ_{eq}. Since χ is temperature dependent, equilibrium swelling ratio λ_{eq} also depends on temperature, which is actually given by Fig. S1, showing the relation between temperature and equilibrium swelling ratio λ_{eq}. Combined with Eq. (S1) (showing the relation between equilibrium swelling ratio λ_{eq} and interaction parameter χ), the temperature-χ relationship could be obtained. In our simulations, different χ values were assigned to different sections (e.g., Fig. 3(d, f) and 4(d, f, h)).

As an example, a 5-layer model was used for the simulation in Fig. 2(b). From top to bottom, the 1st layer is a 0.5 mm-thick hydrogel with χ = 0.378 modeled by 14,400 three-dimensional coupled displacement-temperature elements (C3D8T). The 2nd layer is a 2.5 μm-thick PI with modulus 3.2 GPa and Poisson's ratio 0.34 modeled with 3,916 C3D8T elements. The 3rd layer was a 400 nm-thick Au electrode with modulus 79 GPa and Poisson's ratio 0.44 modeled by 4,698 C3D8T elements. The 4th layer was the same as the 2nd layer. The 5th layer is the same as the 1st layer. The length and width of all the layers were 6 mm and 2 mm, respectively. Adjacent layers were tied together.

FEM simulations were also used to study the temperature distributions. The PI layers were neglected due to their very small thickness (5 μm) compared to that of the whole structure (1 mm) shown in Figure S3. The hydrogel with thickness 1 mm was on top of a glass substrate (60 mm × 60 mm × 1.2 mm), and both were modeled via the solid element

DC3D8 in the commercial finite element package ABAQUS. The heater mesh, modeled by the shell element DS4 with thickness 400 nm, was at the mid-surface of the hydrogel along the thickness direction (1 mm). Natural convection with the coefficient of heat convection h = 25 Watt /(m^2·K)[3] was applied at the outer boundary. The thermal conductivity, mass density and thermal capacity of Au were 317 Watt /(m·K), 19300 Kg/m^3 and 129 J/(Kg·K) [3], respectively; for hydrogel, thermal conductivity 0.6 Watt /(m·K), mass density 1112 Kg/m^3 and thermal capacity 2375 J/(Kg·K) [4]; for glass, thermal conductivity 1.1 Watt /(m·K)[5], mass density 2500 Kg/m^3 and thermal capacity 750 J/(Kg·K) [3]. For 0.32 W applied to the heater mesh in the experiment, the temperature distribution at time of 135 s is shown in Figure S4. The temperature over majority part of the hydrogel is approximately uniform and is slightly higher than 40 ^{o}C with the average value of 45.6 ^{o}C.

Figure S7 shows the temperature distribution in the hemispherical shell shaped pNIPAM hydrogel after heating obtained by the finite element method. The hemispherical shell described in Figure S6 is located on a glass slide, and their inside space is filled with water (thermal conductivity 0.6 Watt /(m·K), mass density 1003 Kg/m^3, and thermal capacity of 4179 J/(Kg·K)[3]. The second and the third circular heaters were heated with power of 0.0819 W and 0.239 W, respectively, in the experiment; and the outer boundary was considered as natural convection with coefficient of convection 25 Watt /(m^2·K) [3]. Figure S7 shows the temperature distribution of the system at time of 120 s, in which the temperature (around 37 ^{o}C) of two sections with heating are clearly higher than that (below 33 ^{o}C) of other sections.

SI References

[1] W. Hong, X. H. Zhao, J. X. Zhou, Z. G. Suo, *J Mech. Phys. Solids* **2008**, 56, 1779.

[2] Z. Duan, Y. An, J. Zhang, H. Jiang, *Acta Mech. Sinica* **2012**, 28, 1058.

[3] F.P. Incropera, D.P. Dewitt, T.L. Bergman, A.S. Lavine, Fundamentals of heat and mass transfer (Eds: J. Hayton), John Wiley & Sons, New York **2006**.

[4] N.S. Satarkar, S.A. Meenach, K.W. Anderson, and J.Z. Hilt, *AICHE J*. **2011**, 57, 852.

[5] H. Kim, E. Brueckner, J. Song, Y. Li, S. Kim, C. Lu, J. Sulkin, K. Choquette, Y. Huang, R. G. Nuzzo, and J. A. Rogers, *Proc. Natl. Acad. Sci. USA* **2011**, 108, 10072.

SI Figure Captions

Figure S1. The LCST of the pNIPAM hydrogel is around 32-34 ^{o}C. The deswell ratio is greater than 35%.

Figure S2. (a) Design of a stretchable/compressible heater mesh, with overall size of 11.3 mm X 9.3 mm. (b) Detailed planar dimensions of the mesh, including the PI layers and metal parts. (c) Schematic cross sectional illustration of the mesh, including 5/400 nm Cr/Au sandwiched by two layers of 2.5 μm PI.

Figure S3. (a) Schematic cross sectional illustration of a 5 layer model used for the 1 mm thick hydrogel with heater mesh embedded in the middle. (b) Strain distribution in the mesh after applying 13% compressive thermal strain to the hydrogel.

Figure S4. FEM simulation results for the temperature distribution of the hydrogel when heated by a heater mesh. (a) Temperature distribution in the hydrogel and the supporting glass substrate during heated by the mesh. The glass substrate acts as a heat sink. (b) Detailed temperature information in each layer. The average temperature in the hydrogel is around 45.6 ^{o}C, which is sufficient to trigger the hydrogel to deswell.

Figure S5. (a) Schematic illustration of a hemispherical shell hydrogel. The shell thickness is 1 mm, and its outer and inner diamters are 8 mm and 7 mm, respectively. (b) Optical image of a circular heater mesh that conforms onto a convex mold after retrieval from water. The inset picture shows an magnified view of the mesh conforming to the mold. (c) Optical image of a hydrogel with mesh embedded while confined by two molds during the fabrication procedure.

Figure S6. (a) Optical image of a hemispherical shell made of hydrogel with embedded, concentric circular heaters. Shape programming of the hydrogel after switching on the heaters 1 and 2 (b); 2 and 3 (c); 3 and 4 (d); 4 and 5 (d).

Figure S7. FEM simulation results for the temperature distribution of the hemishperical shell hydrogel due to activation of heaters 2 and 3. (a) Temperature distribution in the hydrogel and the supporting glass substrate after activating the heater mesh for 2 minutes. (b) Detailed temperature mapping in the layers of top hydrogel shell, heater mesh, and bottom hydrogel shell.

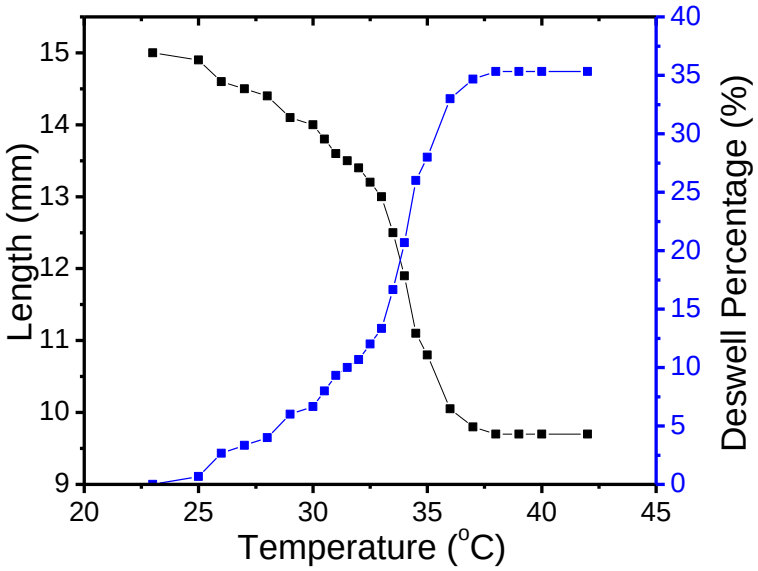
Length (mm)
Deswell Percentage (%)
Temperature (°C)
15
14
13
12
11
10
9
40
35
30
25
20
15
10
5
0
20
25
30
35
40
45

Figure S1

(a)

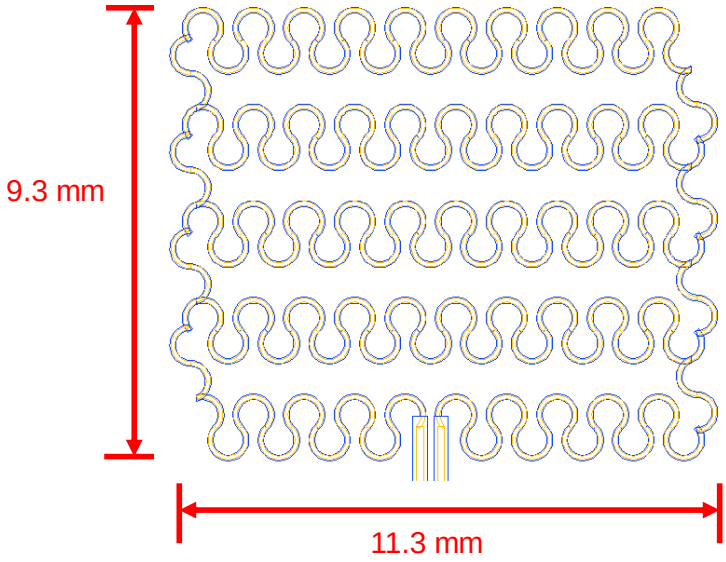
9.3 mm
11.3 mm

(b)

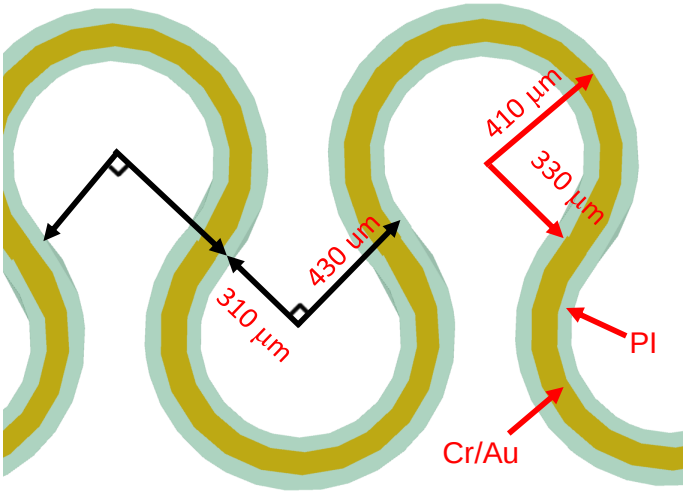
410 μm
330 μm
430 μm
310 μm
PI
Cr/Au

(c)


Cr/Au
5/400 nm
PI 2.5 μm
PI 2.5 μm

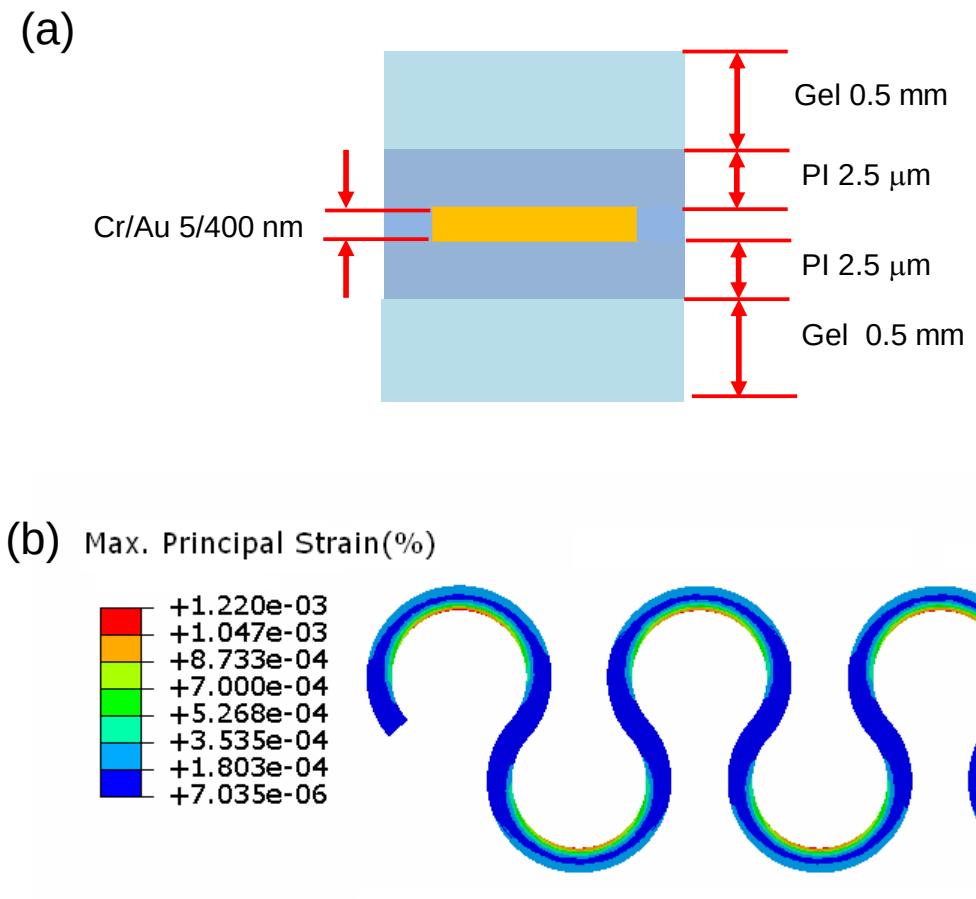
(a)
Gel 0.5 mm
PI 2.5 μm
Cr/Au 5/400 nm
PI 2.5 μm
Gel 0.5 mm
(b) Max. Principal Strain(%)
+1.220e-03
+1.047e-03
+8.733e-04
+7.000e-04
+5.268e-04
+3.535e-04
+1.803e-04
+7.035e-06

Figure S3

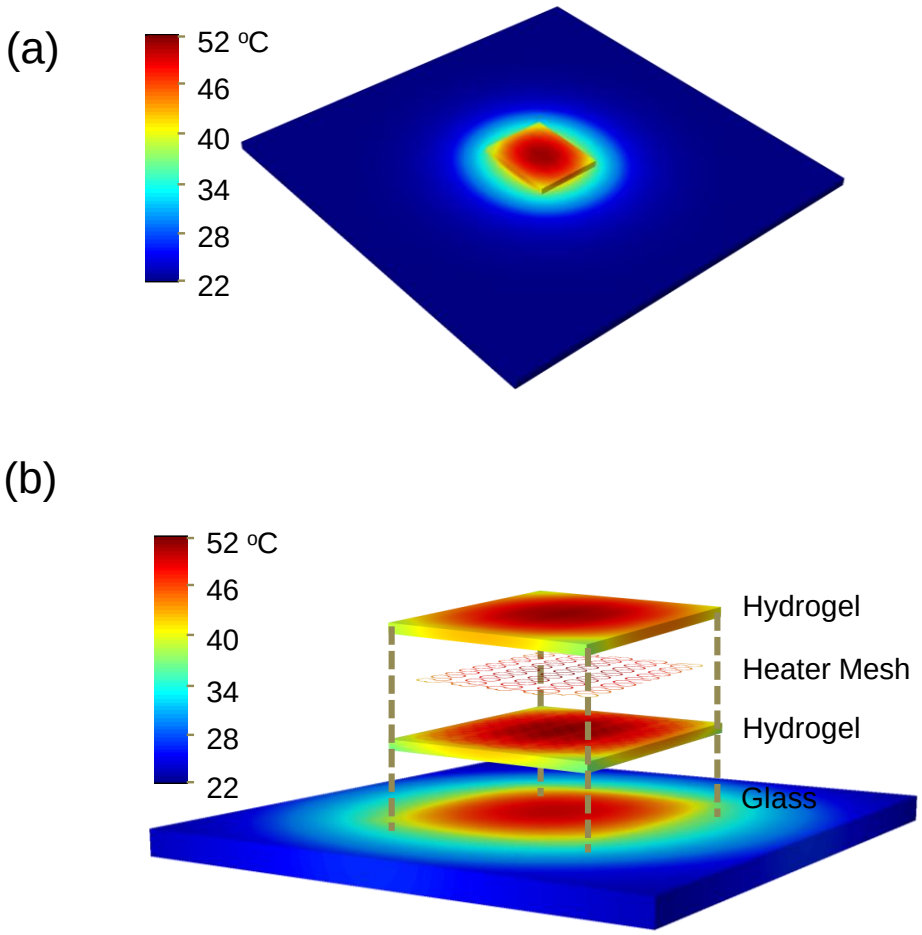
(a)
52 °C
46
40
34
28
22
(b)
52 °C
46
40
34
28
22
Hydrogel
Heater Mesh
Hydrogel
Glass

Figure S4

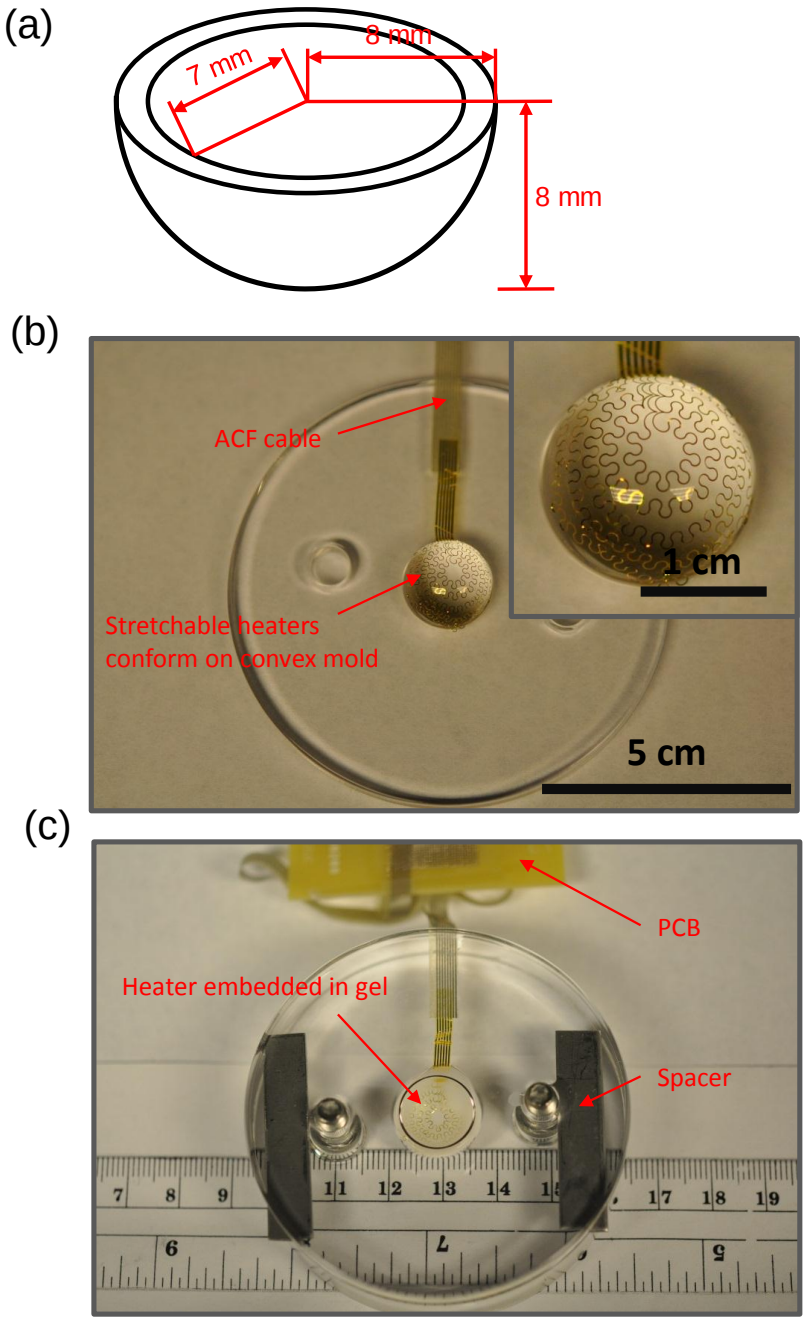
(a)
7 mm
8 mm
8 mm
(b)
ACF cable
Stretchable heaters
conform on convex mold
1 cm
5 cm
(c)
PCB
Heater embedded in gel
Spacer

Figure S5

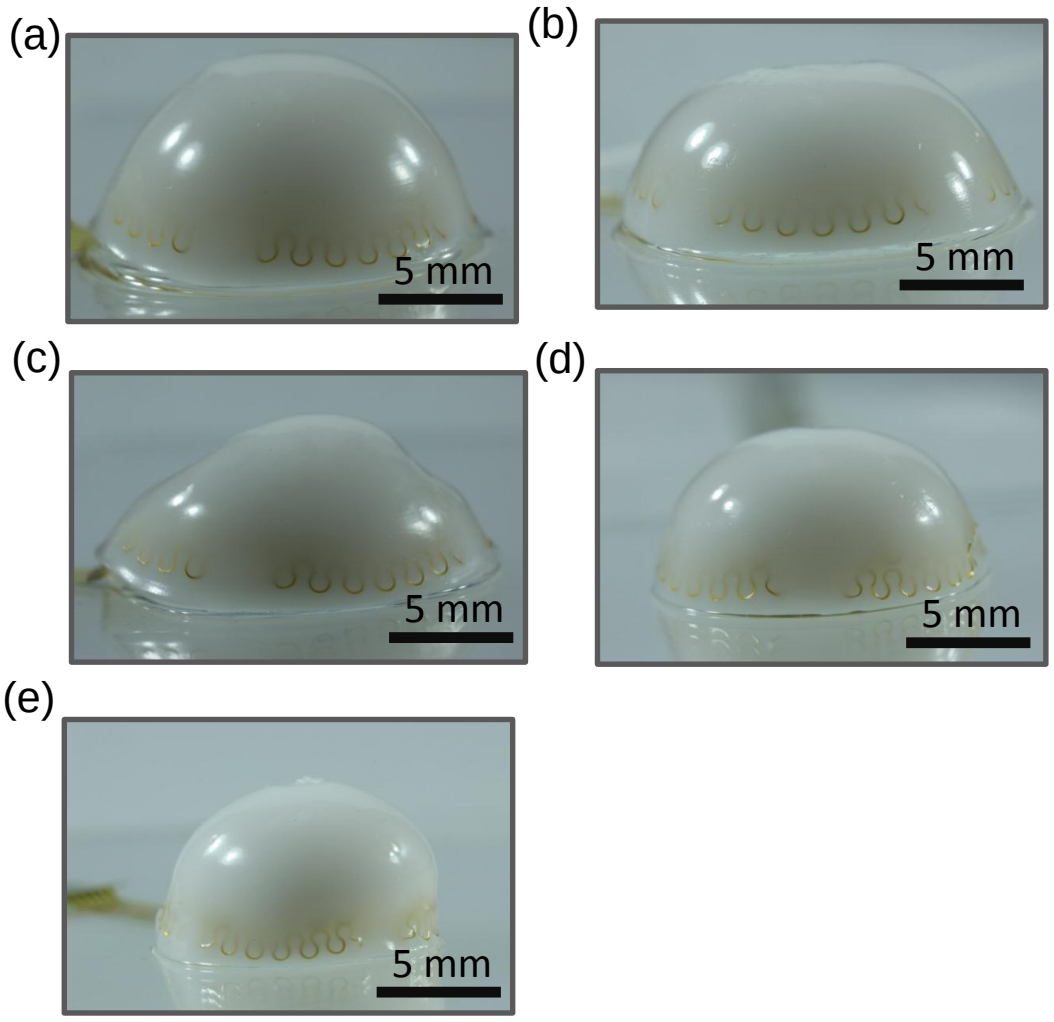

Figure S6

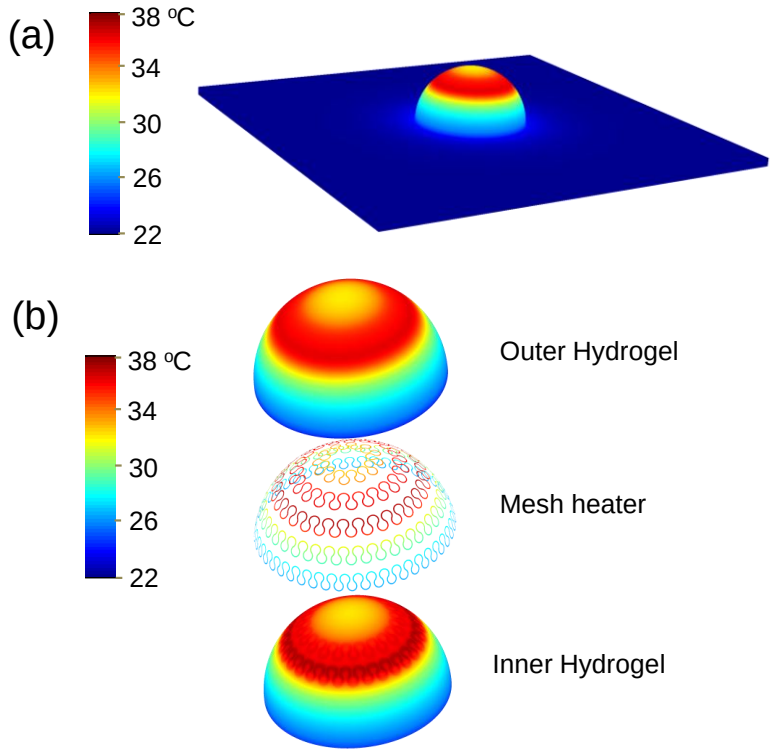
(a)
38 °C
34
30
26
22
(b)
38 °C
34
30
26
22
Outer Hydrogel
Mesh heater
Inner Hydrogel

Figure S7